This paper is available online at www.praiseworthyprize.org
International Journal on Engineering Applications (I.R.E.A.), Vol. 11, N. 1
ISSN 2281-2881
January 2023

Simulation and Numerical Investigation of the Effect of Temperature and Defect on ZnTe/ZnSe/ZnO Thin-Film Photovoltaic Solar Cell Performance Efficiency

Samer H. Zyoud[1, 2], Ahed H. Zyoud[3]

Abstract – *Thin film-based solar cell semiconductor emerges as a promising candidate for solar photovoltaic future applications. A proposed heterojunction ZnTe/ZnSe/ZnO thin film-based solar cell has been simulated by using Solar Cell Capacitance Simulator-One Dimension (SCAPS-1D) in order to study the impact of temperature and defect layers on its efficiency parameters. The heterojunction thin film-based solar cell has been selected for simulation due to its low cost, availability, and reduced toxicity compared to other absorber layer materials. Numerical modeling has been used to comprehend device properties before fabrication. The results indicate that the efficiency parameters (J_{sc}, V_{OC}, FF, and η) have been significantly affected by temperature and the presence of defect layers. The simulated J-V characteristics demonstrate how defect density affects solar cell efficiency parameters. In the defect system, the efficacy parameters have been reduced except for a slight increase in V_{OC} at 300 K. The findings of this study are significant as they demonstrate the importance of understanding the impact of temperature and defect layers on the performance of thin film-based solar cells. The use of numerical modeling tools like SCAPS-1D can aid in the design and development of new solar cell technologies, which could ultimately lead to the widespread adoption of solar energy as a clean and sustainable energy source.* ***Copyright © 2023 The Authors.***
Published by Praise Worthy Prize S.r.l.. This article is open access published under the CC BY-NC-ND license (http://creativecommons.org/licenses/by-nc-nd/3.0/).

Keywords: *Thin Film Solar Cell, ZnTe/ZnSe/ZnO, SCAPS-1D, Defect, Bandgap*

Nomenclature

A	Area
CB	Conductance Band
D	Diffusivity of the minority carrier
e	Charge (1.6×10^{-19} C)
E_C	Conductance energy
E_F	Fermi energy
E_g	Bandgap
E_{G0}	Extrapolated bandgap at absolute zero
E_V	Valance Energy
E_t	Total defect energy
FF	Fill Factor
G	Generation rate
h	Blank constant
I_o	Maximum current
I_S	Saturation current
I_{SC}	Short-circuit current
J_n	Electron current densities
J_p	Hole current densities
J_{SC}	Short-circuit current density
k	Constant
L	Diffusion length of the minority carrier
MO	Molybdenum
m_e^*	Effective electron mass
m_h^*	Effective hole mass
n	Electrons concentration
N_A	Charged impurities of acceptor
N_C	CB effective density of states
N_D	Charged impurities of donor
N_V	VB effective density of states
p	Holes concentration
PV	Photovoltaic
q	Electron charge
$QE\%$	Quantum Efficiency percent
R	Recombination rate
SCAPS-1D	Solar Cell Capacitance Simulator in 1 Dimension
SnO_2	Tin(IV) oxide
n_i	Intrinsic carrier concentration
T	Temperature
VB	Valance Band
V_{OC}	Open-Circuit voltage
$V_{e\text{-}th}$	Electron thermal velocity
$V_{p\text{-}th}$	Hole thermal velocity
W	Thickness
ZnSe	Zinc Selenide
ZnTe	Zinc Telluride
ZnO	Zinc Oxide
η	Efficiency

Copyright © 2023 The Authors. Published by Praise Worthy Prize S.r.l.
This article is open access published under the CC BY-NC-ND license (http://creativecommons.org/licenses/by-nc-nd/3.0/)
Available online by January 31st, 2023
https://doi.org/10.15866/irea.v11i1.20839

λ	Wavelength
Ψ	Electrostatic potential
ε_o	Vacuum permittivity
ε_r	Relative permittivity
ε_r	Dielectric permittivity (relative)
μ_e	Electron mobility
μ_p	Hole mobility
ρ_p	Holes distribution
ρ_n	Electrons distribution
χ_e	Electron affinity

I. Introduction

Studying the effect of temperature on hetero-junction thin-film solar cells is one of the emerging issues in photovoltaic applications. Exposing the solar panels to direct sunlight will lead to an increase in their operating temperature, and the solar panels may be heated to a higher temperature. In addition, the photovoltaic thin-film solar cells under concentrated light are potentially interesting in the research and in the applications. Using giant lenses or mirrors to concentrate the sunlight on a small area of the photovoltaic solar cell will increase the efficiency of converting light to electricity by using a minimum amount of the solar cell devices materials. This technology will produce increases in the thin-film solar cell devices temperature. In addition, solar cell panels used in a spacecraft will increase the solar cell panel temperature [1], [2]. This increase in temperature may affect the solar cell device's efficiency. The computational simulation will consider the impact of operating temperature on solar panel efficiency. Typically, higher temperatures negatively affect the photovoltaic efficiency of solar cells, resulting in a reduction in overall cell efficiency [3].

The performance of solar cells is highly dependent on their operating temperature, which is one of the most important factors affecting their overall efficiency. The impact of temperature on solar cell efficiency parameters, such as open-circuit voltage (V_{OC}), short-circuit current density (J_{SC}), Fill Factor (*FF*), efficiency (η%), and Quantum Efficiency percent (QE%), is well documented.

Changes in operating temperature can significantly influence these parameters, resulting in a reduction in the overall efficiency of the solar cell device.

Therefore, understanding the impact of temperature on solar cell performance is crucial in designing and developing more efficient solar cell technologies [3]. An increase in operating temperature generally leads to an increase in reverse saturation current. Additionally, operating temperature can also affect open-circuit voltage (V_{OC}), which tends to decrease as saturation current increases. At higher temperatures, electrons in the solar cell gain more energy, leading to faster recombination with holes before they reach the depletion region and are collected. This can result in reduced solar cell efficiency and stability. Therefore, careful consideration of operating temperature is necessary when designing and developing solar cell technologies in order to ensure their optimal performance and stability [4], [5]. In addition to the factors mentioned previously, solar cell efficiency decreases as operating temperature increases due to the reduction in the band gap of most semiconductor materials. This reduction negatively affects electron and hole mobility, carrier concentrations, and bandgaps of the material, leading to a decrease in the overall efficiency of the solar cell.

Numerical simulation is an essential tool for the design and the optimization of solar cells. It allows researchers to investigate the impact of various factors, such as material properties, geometry, and operating conditions, on the performance of solar cells. This approach offers a cost-effective and efficient method for evaluating the feasibility of novel solar cell designs and identifying potential areas for improvement [6]-[10]. In order to understand better the impact of operating temperature on solar cell efficiency, researchers use simulation programs such as SCAPS-1D. It is a one-dimensional solar cell simulation program developed by a research group at the University of Gent. It provides valuable insights into the effect of different factors, including temperature and defects, on solar cell efficiency parameters. By using such simulation tools, researchers can optimize the design and performance of solar cell devices for various operating conditions [11]-[14].

Zyouds have used SCAPS-1D to simulate the optimization of the ZnTe-based thin-film heterojunction solar cells via the replacement of metal chalcogenide buffer layers, and Effect of absorber (acceptor) and buffer (donor) layers thickness on Mo/Cdte/Cds/ITO thin film solar cell performance: SCAPS-1D simulation aspect [15]-[17].

The SCAPS-1D program will be utilized to evaluate numerically the photovoltaic device's efficiency performance at various operating temperatures ranging from 280 to 420 K. Additionally, SCAPS-1D will be employed to simulate the effect of a neutral defect in the absorber ZnTe layer on cell performance at an operating temperature of 300 K [18]. The suggested heterojunction solar cell device ZnTe/ZnSe/ZnO has been chosen based on literature reports of successfully prepared and studied devices. SCAPS-1D has been used in this study in order to gain a better understanding of the impact of temperature and defects on solar cell performance, which can aid in the development of more efficient and stable solar cell technologies [19], [20]. The device performance efficiency will be observed as a function of efficiency parameters (V_{OC}, J_{SC}, *FF*%, η%, and *QE*%).

The rest of the paper is organized as follows. Section II shows the numerical modeling and the material parameters. This section will describe the methodology of the device simulation and modeling, the input parameters, and the used mathematical equations. Section III represents the results and the discussion details with subtitles such as Effect of working temperature on the device performance, Effect of deep defect in layers on solar cell performance. Finally, the conclusion is presented in the final section of this paper.

Copyright © 2023 The Authors. Published by Praise Worthy Prize S.r.l.

II. Numerical Modeling and Material Parameters

Numerical modeling has been employed to offer a theoretical road map for speedy experimental optimization of processes. Simulation has been used for the optimization of parameters in energy [21], [22], transportation [23]-[25], heat transfer [26]-[28], production planning [29], water, and food production [6], [30]. Numerical simulation has also been employed in improving the properties of solar cells [14], [31], [32].

Nanostructured metal oxide is among the emerging solar cells. Modeling of nanostructured metal oxide interest has increased significantly for decades due to the simplicity and ease of manipulation of the tool [33], [34].

The modeling techniques are used to compute the fundamental physical properties such as holes and electrons concentration and electrical potential. It also provides more information regarding the influence of material physical parameters on device functional parameters or characteristics. For the numerical modeling of solar cells, physical parameters of material are taken as input for the simulation software [35].

II.1. Numerical Modeling

The SCAPS-1D simulation software has been used here to calculate the suggested device simulating results.

The software can solve basic semiconducting equations for electron-hole based on Poisson's Equations (1), (2) [13], [36]:

$$\frac{d^2\Psi}{dx^2} = \frac{e}{\epsilon_o\epsilon_r}[p(x) - n(x) + N_D - N_A + \rho_P - \rho_n] \quad (1)$$

where Ψ is the electrostatic potential, e is the electrical charge, ϵ_r is relative, ε_o is the vacuum permittivity, p and n are the holes and electrons concentration, N_D is the charged impurities of donor, N_A is the charged impurities of acceptor, ρ_p is the holes distribution, and ρ_n is the electrons distribution. The continuity equations for electrons and holes are:

$$\frac{dJ_n}{dx} = \frac{dJ_p}{dx} = G - R \quad (2)$$

where J_n is the electron current densities, J_p is the hole current densities, R is the recombination rate, and G is the generation rate. The electron current densities and the hole current densities produced by drift and diffusion are representing the carrier transport in semiconductors. The electron current densities J_n can be expressed as:

$$J_n = D_n\frac{dn}{dx} + \mu_n n\frac{d\varphi}{dx} \quad (3)$$

The holes current densities J_p can be presented as:

$$J_p = D_p\frac{dp}{dx} + \mu_p p\frac{d\varphi}{dx} \quad (4)$$

The open-circuit voltage originally decreases with increasing temperature because of the temperature dependence of the I_o [37]:

$$I_o = qA\frac{Dn_i^2}{LN_D} \quad (5)$$

where D is the diffusivity of the minority carrier, L is the diffusion length of the minority carrier, N_D is the doping, and n_i is the intrinsic carrier concentration. The intrinsic carrier concentration (n_i) is the most significantly affected by temperature among the above parameters:

$$n_i^2 = 4\left(\frac{2\pi kT}{h^2}\right)^3 (m_e^* m_h^*)^{3/2} e^{-\frac{E_{G0}}{kT}} = BT^3 e^{-\frac{E_{G0}}{kT}} \quad (6)$$

where T is the temperature, B is the independently temperature constant, E_{G0} is the extrapolated bandgap at absolute zero, m_e^* is the density of states effective masses of electrons, m_h^* is the density of states effective masses of holes. In addition, k is a constant. Replacing n_i equation in I_o equation will prduce the impact of temperature on the V_{OC} as:

$$V_{OC} = \frac{kT}{q}\ln\frac{I_{SC}}{I_O} \quad (7)$$

The Fill Factor (FF) is used to measure a photovoltaic cell quality, which is derived by equating the maximum power (P_{max}) to the theoretical power (P_t), where the theoretical power (P_t) is the open circuit voltage (V_{OC}) multiplied by the short-circuit current density (J_{sc}). FF is given by Equation (8):

$$FF = \frac{V_{max}I_{\max}}{V_{OC}I_{SC}} \quad (8)$$

Energy conversion efficiency is the most frequently used parameter to relate the performance of two solar cells and it is termed as η. It is defined as the ratio of output power from a solar cell to the input power that reaches in from the sun [38] and is expressed by Equation (9) [39]:

$$\eta = \frac{V_{OC} \times J_{SC} \times FF}{P_{in}} \quad (9)$$

Energy conversion efficiency (η) depends on the parameters like incident sunlight intensity, solar cell working temperature, and spectrum type. Therefore, in order to compare two or more solar cells, it is important to control carefully the conditions under which η are measured. The incident light (photons) illumination is AM1.5G spectra through the calculation of the J–V characteristics in this numerical simulation analysis [40].

The input power, P_{in}, from the sun is considered as 1000 W/m^2. The quantum efficiency (QE) is the ratio of the extracted free charge carriers by the solar cell to the

Copyright © 2023 The Authors. Published by Praise Worthy Prize S.r.l.

number of incident photons. In other words, QE relates to the response of a solar cell to different wavelengths. It may be given either as a function of energy or wavelength. The QE will be unity at the precise wavelength if all certain wavelength photons are absorbed and the resulting minority carriers are collected.

The spectral response has been evaluated based on the quantum efficiency measurements. QE is defined according to Equation (10) [41]:

$$QE(\lambda) = \frac{I(\lambda)/q}{\varphi_p(\lambda)} \tag{10}$$

where q is the elementary electrical charge, $I(\lambda)$ is the photogenerated current $\varphi_p(\lambda)$ is the photon flow.

II.2. The Suggested Thin-Film Solar Cell Device Structure

It has been proposed to construct a thin-film solar cell device using a glass substrate as a supporting slide. A molybdenum thin layer film would be deposited on the glass substrate, followed by a ZnTe layer (p-type) with a thickness of 2400 nm on top of the molybdenum layer. A ZnSe layer (n-type) with a thickness of 25 nm would be used as a buffer layer, and a ZnO layer (n-type) with a thickness of 10 nm would be used as a window layer. The selection of materials for the simulation calculations has been based on their efficiency, stability, material cost, and ease of preparation. Fig. 1 illustrates the arrangement of the modeling layers.

II.3. Simulation Input Parameters

The required input parameters used for the suggested thin-film solar cell device are shown in Table I and Table II. The input results have been chosen based on the literature optimal findings [42]-[48].

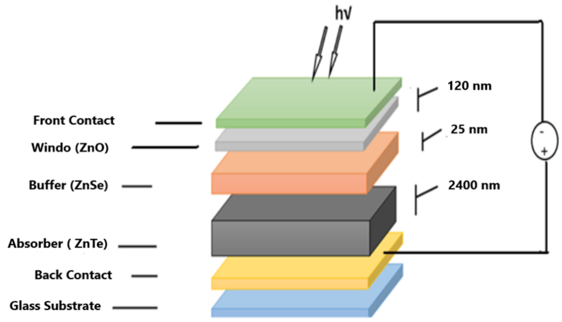

Fig. 1. Schematic structure of a thin film- based solar cell

TABLE I
NECESSARY INPUT PARAMETERS THAT USED FOR THE SUGGESTED THIN-FILM SOLAR CELL DEVICE

Parameters	p -ZnTe	n- ZnSe	ZnO
Thickness (nm)	2400	25	120
Bandgap (eV)	2.26	2.9	3.3
Electron affinity (eV)	3.5	4.09	4.35
Dielectric permittivity (relative)	9.67	10	9
CB effective density of states (cm^{-3})	7×10^{16}	1.5×10^{18}	2.2×10^{18}
VB effective density of states (cm^{-3})	2×10^{19}	1.8×10^{18}	1.8×10^{19}
Electron thermal velocity (cm/s)	1×10^{7}	1×10^{7}	1×10^{7}
Hole thermal velocity (cm/s)	1×10^{7}	1×10^{7}	1×10^{7}
Electron mobility (cm^2/Vs)	330	50	100
Hole mobility (cm^2/Vs)	80	20	25
Donor density ND (cm^{-3})	0	2.5×10^{17}	4×10^{18}
Acceptor density Na (cm^{-3})	5.5×10^{16}	0	0

TABLE II
ELECTRICAL AND OPTICAL PROPERTIES OF BACK AND FRONT CONTACT USED IN SCAPS SIMULATION

Electrical Properties		Back contact	Front contact
Thermionic emission surface recombination velocity (cm/s)	Electron	1×10^{7}	1×10^{7}
	Holes	1×10^{7}	1×10^{7}
Metal work function (eV)		4.625	4.1
Majority carrier barrier height (eV)	Relative to E_F	0.4	0.1
	Relative to E_V or E_C	- 0.0682	0.0571
Allow contact tunneling	Effective mass of electron	1	1
	Effective mass of holes	1	1
Optical Properties	Filter Mod	Reflection	Transmission
	Filter value	0.8	0.95
	Complement of filter value	0.2	0.05

TABLE III
BULK DEFECTS PROPERTIES IN ZNTE/ZNSE/ZNO DEVICE.

Defect	Absorber Layer (ZnTe)	Buffer layer (ZnSe)	Window layer (ZnO)
Charge type	Neutral	Neutral	Neutral
Total density (cm^{-3}): Uniform	1.1×10^{14}	5.0×10^{16}	1.0×10^{16}
Energy distribution: Gauss	E_t = 0.6 eV above EV	E_t = 1.2 eV above EV	Et = 1.65 eV above EV
	E_{kar} = 0.1 eV	E_{kar} = 0.1 eV	E_{kar} = 0.1 eV
Capture cross section area of electrons (cm^2)	1.0×10^{-13}	1.0×10^{-15}	1.0×10^{-15}
Capture cross section area of holes (cm^2)	1.0×10^{-15}	5.0×10^{-13}	5.0×10^{-13}

Copyright © 2023 The Authors. Published by Praise Worthy Prize S.r.l.

The effect of defect on the device layers has been investigated. The defect is supposed to be in the absorber (ZnTe) layer, buffer (ZnSe) layer, and window (ZnO) layer as shown in Table III.

III. Results and Discussion

III.1. Effect of Working Temperature on the Device Performance

A crucial factor that affects the performance and the applications of thin-film solar cell devices is their operating temperature. When exposed to high levels of solar radiation, the temperature of the panels may exceed 300 K, which can have a detrimental effect on the performance of the photovoltaic cells. Therefore, the impact of temperature on the proposed cell has been investigated, and for this purpose, a temperature range of 280-400 K has been considered.

III.1.1. The Effect of Operating Temperature on J-V Characteristics

Fig. 2 depicts the simulated J-V curves for the defect system at temperatures ranging from 280 K to 420 K.

Meanwhile, Figs. 3 present the solar cell efficiency parameters. The results in Figs. 3 illustrate the impact of temperature on various cell efficiency parameters, including V_{OC}, J_{SC}, FF%, and η%. As shown in Fig. 3(a), the V_{OC} value of the thin-film solar cell devices decreases as the temperature increases. This decrease in V_{OC} values is mainly due to the temperature-dependent reverse saturation current (I_s) [49]. The intrinsic carrier concentration (n_i) also contributes to the decrease in V_{OC} with operating temperature. As the temperature increases, the number of thermally generated intrinsic carriers' increases, which leads to a higher concentration of charge carriers in the material. This increased carrier concentration reduces the potential difference across the solar cell, which results in a decrease in V_{OC}. Therefore, the reduction in V_{OC} with operating temperature is due to a combination of factors, including the temperature-dependent reverse saturation current (I_s) and the intrinsic carrier concentration (n_i).) [50], [51]. Fig. 3(b) indicates that the J_{SC} is not significantly affected by changes in temperature. Meanwhile, the FF decreases slightly (with no significant change observed) with an increase in temperature, as shown in Fig. 3(c). The efficiency (η) of thin-film solar cell structures also decreases with increasing temperature, as depicted in Fig. 3(d). At higher temperatures, various parameters such as electron and hole motilities, carrier concentrations, and band gaps of the materials are affected. The band gap is directly influenced by the temperature, and it increases with temperature, contributing to the decrease in cell efficiency [40]. This will result in a lowering in the cell efficiency [52]. The bandgap of the absorber layer in thin-film solar cell devices is typically narrow. This narrow bandgap can facilitate electron-hole pair recombination, which can decrease the cell efficiency.

This behavior can be attributed to the increase in interatomic spacing that occurs when the amplitude of atomic vibrations increases due to the increased thermal energy. The effect of temperature on interatomic spacing is quantified by the material's linear expansion coefficient.

As a result, the performance of thin-film solar cell devices decreases at higher temperatures, as shown in Fig. 2.

III.1.2. The Influence of Temperature on the Energy Band Gap

The band alignment between the layers of a solar cell device is crucial for efficient current transport and performance. The SCAPS-1D software program can be used to simulate and calculate the band diagram of the solar cell structure. Fig. 4 shows the band diagram of the proposed device, with the ZnTe layer (0-2400 nm), ZnSe layer (2400-2425 nm), and ZnO layer (2425-2540 nm).

The band diagram indicates good alignment between the absorber, the buffer, and the window layers, as shown in Fig. 5(a). The band diagram also reveals four recombination regions: recombination at the ZnTe layer back contact (region R1), bulk recombination in the absorber ZnTe layer (region R2), space charge depletion layer in ZnTe (region R3), and absorber/buffer interface recombination (region R4). A thin absorber layer can reduce the distance of the bulk recombination region in the ZnTe absorber layer (region R2) and keep the back contact close to the depletion region (R3), leading to increased recombination at the back contact. As a result, a significant amount of photogenerated carriers is recombined at the back contact, reducing the device's efficiency. The optical inventory factor is related to the absorption coefficient and the thickness of the active layer. An increase in temperature causes a decrease in the refractive index of the semiconductor, leading to a decrease in the optical inventory factor and, consequently, a decrease in the absorption coefficient. This decrease in absorption coefficient results in a decrease in the number of absorbed photons and a decrease in the number of generated electron-hole pairs, which leads to a decrease in the short-circuit current density (J_{SC}) and, consequently, a decrease in the overall efficiency of the thin-film solar cell device [53], [54].

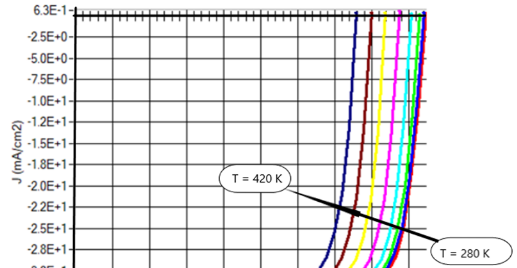

Fig. 2. Current mode with voltages

Copyright © 2023 The Authors. Published by Praise Worthy Prize S.r.l.

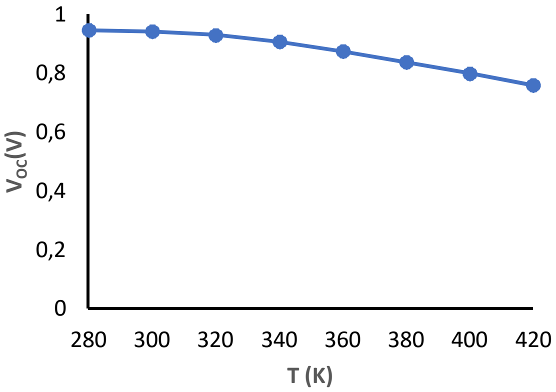

(a)

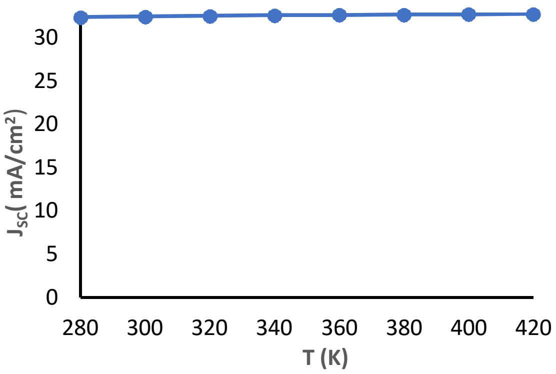

(b)

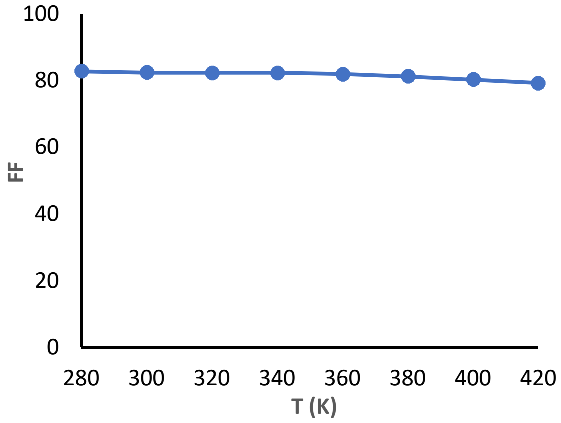

(c)

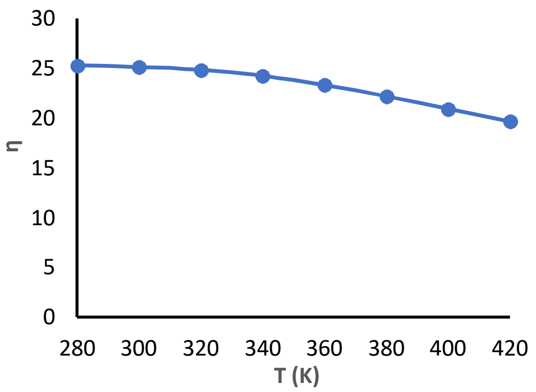

(d)

Figs. 3. Solar cell operating characteristics at different operatin temperatures, (a) V_{OC}, (b) J_{SC}, (c) FF, and (d) η

Figs. 5(a)-(c) illustrate the band diagram at different temperatures. When the photons have an energy higher than the energy bandgap (E_g) of the semiconductor materials, the photons will be absorbed and generate electron-hole pairs [55]. The cut-off wavelength of photons that can generate carriers in a semiconductor is dependent on the bandgap energy, and this energy is temperature-dependent. Equations (11) and (12) can be used to define the relationship between the bandgap energy and temperature [56]:

$$\lambda_g \text{ (nm)} = \frac{1240}{E_g(eV)} \tag{11}$$

$$E_g(T) = E_g(0) - \frac{\alpha T^2}{T + \beta} \tag{12}$$

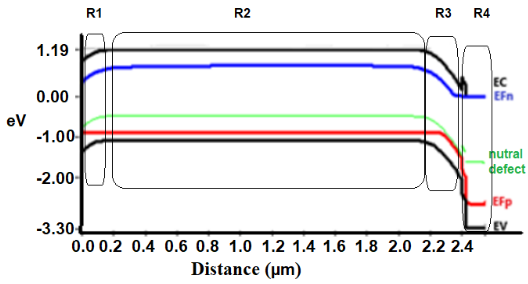

Fig. 4. Band diagram for thin film structure solar cells, at T = 300 K

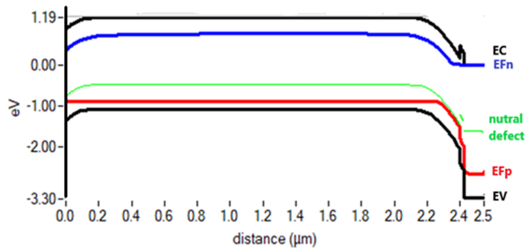

(a) T= 300 K

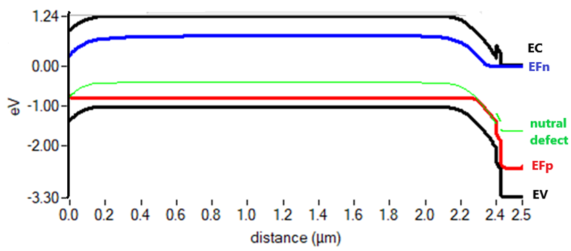

(b) T= 350 K

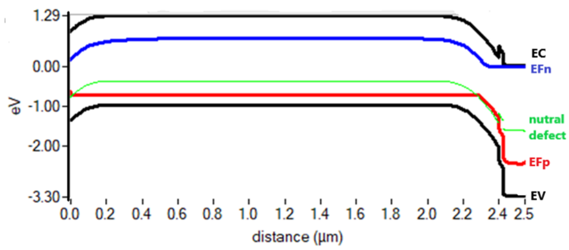

(c) T=400 K

Figs. 5. Band diagram for thin film structure solar cells at different temperature, (a) T = 300 K, (b) T = 350 K, (c) T = 400 K

Copyright © 2023 The Authors. Published by Praise Worthy Prize S.r.l.

The variable $E_g(T)$ denotes the energy of the bandgap at certain temperatures, while $E_g(0)$ is the bandgap energy of the semiconductor at approximately 0 K. The constants α and β are used in the calculation of the bandgap energy.

Table IV shows the bandgap energy values of the absorber (ZnTe), buffer (ZnSe), and window (ZnO) layers as a function of temperature.

III.1.3. The Influence of Temperature on the Quantum Efficiency Percent (QE%)

Fig. 6 presents the quantum efficiency percent (*QE*%) profiles at different temperature values, which have been obtained through calculations by using the SCAPS-1D software program. These profiles exhibit a peak response to illumination wavelength, with a range of 80-90% *QE*% in the wavelength range of 520-800 nm. However, the *QE*% starts to decrease at a threshold limit of 400 nm, with a value of 15%.

This decrease is mainly due to the cut-off edge of the ZnO window layer, in addition to recombination and absorption in the absorber and buffer layers. Within the range of 300-420 K, an increase in temperature does not have a significant effect on *QE*%.

The *QE*% profile displays absorption maxima at approximately 510 nm, which is consistent with the input ZnTe value (2.26 eV). No significant change has been observed in *QE*% with temperature, which can be attributed to the small range of temperatures studied (300-420 K), indicating that a temperature change of 120 °C is not enough to cause a noticeable effect on the semiconductor structure. Additionally, shallow level defects have not appeared in the near band edge region, which may contribute to the lack of significant change in *QE*% [57].

III.2. Effect of Deep Defect in Layers on Solar Cell Performance

Deep-level defects are known to affect significantly the performance of semiconductor devices, including solar cells. In this study, the effects of defects on solar cell performance have been investigated by using the parameters outlined in Table III. It is challenging to manufacture a perfect or ideal semiconductor solar cell thin-film crystal, and most prepared thin-film solar cells have defects.

These defects adversely affect solar cell efficiency by creating new recombination pathways, converting light energy into heat due to electron-hole recombination. They also introduce deep energy levels within the semiconductor bandgap, leading to a degradation in carrier lifetime and quantum efficiency.

Recombination centers are one of the primary reasons for defects, as they trap photogenerated carriers before they reach the solar cell terminals. In order to address these issues, a simulation calculation has been conducted for the proposed thin-film solar cell under a non-defected state, with a simulation temperature of 300 K.

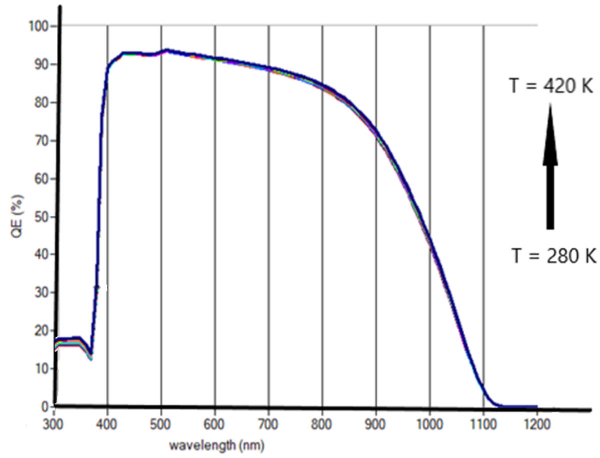

Fig. 6. Quantum efficiency of thin film solar cell at various operating temperature

TABLE IV
BANDGAPS ENERGY WITH DIFFERENT TEMPERATURE DEGREES

T (K)	Bandgap energy (eV) Absorber (ZnTe)	Buffer (ZnSe)	Window (ZnO)
300	2.26	2.9	3.3
350	2.31	2.96	3.35
400	2.36	3.01	3.41

III.2.1. The Effect of Defect on the J-V Characteristic

Fig. 7 shows the J-V characteristic for both defect and ideal crystals at a temperature of T = 300 K. The short circuit density (J_{SC}), fill factor (FF), and quantum efficiency (η) all decrease with defects, while the open-circuit voltage (V_{OC}) is only slightly affected, as shown in Table V.

Deep-level defects mainly act as recombination centers, resulting in increased recombination rates and lower short-circuit currents with higher defect densities.

Higher defect densities also lead to higher series resistance and poorer fill factor, ultimately resulting in a significant drop in efficiency of 2.6% compared to a non-defected system.

The defect density location is theoretically changed from the bottom of the conductivity band to the top of the valence band, with both systems exhibiting approximately similar V_{OC} values. The decrease in efficiency is attributed to recombination with the localized energy levels created by the defects.

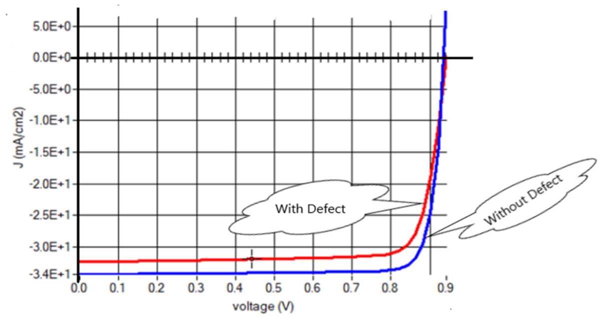

Fig. 7. Current mode with voltage at 375 K

TABLE V
DEFECT DEPENDENCY

	V_{OC} (V)	J_{SC} (mA/cm^2)	FF	η
With Defect	0.9423	32.411912	82.42	25.17
Without Defect	0.9359	34.371902	86.23	27.74

Therefore, it is crucial to control the densities of deep-level defects in real experiments. The decrease in quantum efficiency observed in the defected system has a significant impact on the overall efficiency of the solar cell device, as indicated by Fig. 7 and the data presented in Table V.

This highlights the importance of minimizing the number of defects in the semiconductor layer during manufacturing in order to improve the efficiency of the solar cell. Efforts should be made to produce near-perfect crystal semiconductor layers to achieve optimal solar cell efficiency.

III.2.2. The Effect of Defect on the Band Diagram

The band diagram in Figs. 8(a), (b) illustrates the influence of defects on the band structure and band alignment of 2D materials. These results provide further insights into the potential to modify the band structure of these materials through defect engineering. The Fermi level in the pristine center region is situated roughly midgap, about 0.6 eV above the valence band for ZnTe, 1.2 eV above the valence band for ZnSe, and 1.65 eV above the valence band for ZnO, as shown in Fig. 8(b).

III.2.3. The Effect of Defect on the Quantum Efficiency Percent (QE%) Profiles

The impact of defects on the quantum efficiency of thin-film solar cells was investigated. Figs. 8 show the QE profiles for both perfect and defective crystals, covering a range of illumination from 300-800 nm.

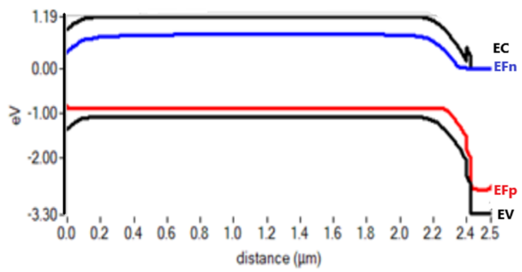

(a) without defect

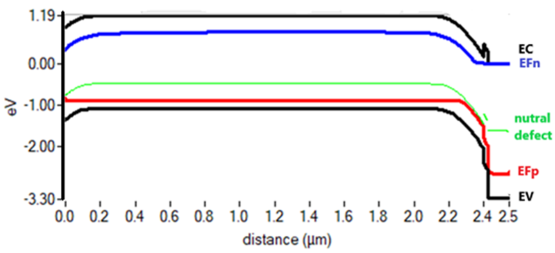

(b) with defect

Figs. 8. Band Diagram, (a) without defect, (b) with defect , at T = 300 K

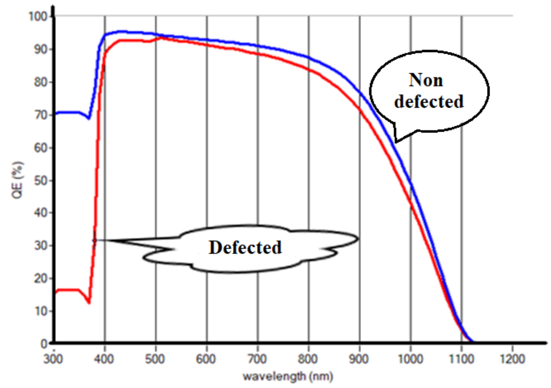

Fig. 9. Quantum efficiency of thin film solar cell at various operating temperature with defect and without defect

It has been observed that the *QE* value of the defective system is lower than that of the perfect crystal system in the 300-520 nm range. This decrease in quantum efficiency caused by defects ultimately leads to lower solar cell device efficiency, as illustrated in Fig. 9 and Table V.

Therefore, manufacturers should consider minimizing the number of defects as much as possible and aim to prepare perfect crystal semiconductor layers to improve and increase solar cell efficiency.

IV. Conclusion

Semiconductor-based thin film solar cells have emerged as a promising option for solar photovoltaic applications. Numerical modeling, such as with the SCAPS-1D tool, can be used to optimize their performance by studying the impact of factors like temperature and defects on efficiency parameters. The simulated ZnTe/ZnSe/ZnO heterojunction thin film solar cell has revealed that the presence of defects and higher temperatures can significantly reduce the device's efficiency and quantum efficiency. This highlights the importance of controlling these factors to design and fabricate high-performance, low-cost, and environmentally safe thin film solar cells. The results of this study indicate that the optimal performance of the ZnTe/ZnSe/ZnO thin film solar cell has been achieved at 280 K, with an efficiency of 25.29%, J_{SC} of 33.64 mA/cm^2, V_{OC} of 1.19 V, and FF of 84.8%. These findings demonstrate the potential for thin film-based solar cells to provide high efficiency and performance, making them a viable option for solar photovoltaic applications.

Furthermore, the study has revealed that the bandgap energy of the thin film solar cell has increased by 1 meV/K as the temperature has increased, emphasizing the importance of controlling the operating temperature to optimize performance. Additionally, defects in the crystal structure of the thin film solar cell system had a significant negative impact on its efficiency and quantum efficiency at higher temperatures. Hence, future research can focus on identifying and mitigating these defects to improve further the performance of thin film solar cells. Overall,

Copyright © 2023 The Authors. Published by Praise Worthy Prize S.r.l.

this research provides insight into the potential of thin film-based solar cells as a cost-effective, sustainable, and eco-friendly energy source that can address the rising demand for clean and renewable energy.

Acknowledgements

We gratefully acknowledge to Dr. Marc Burgelman, University of Gent, Belgium, for providing the SCAPS – 1D simulation software. Furthermore, we are grateful to Ajman University for supporting this study.

References

[1] G.A. Landis, D. Merritt, R.P. Raffaelle, D. Scheiman, *High-temperature solar cell development*, (2005).

[2] D.A. Scheiman, G.A. Landis, V.G. Weizer, High-bandgap solar cells for near-sun missions, in: *AIP Conference Proceedings*, American Institute of Physics, 1999, pp. 616-620.

[3] P. Singh, S. Singh, M. Lal, M. Husain, Temperature dependence of I–V characteristics and performance parameters of silicon solar cell, *Solar Energy Materials and Solar Cells*, 92 (2008) 1611-1616.

[4] S. Wagner, J. Shay, P. Migliorato, H. Kasper, CuInSe2/CdS heterojunction photovoltaic detectors, *Applied Physics Letters*, 25 (1974) 434-435.

[5] P. Chelvanathan, M.I. Hossain, N. Amin, Performance analysis of copper–indium–gallium–diselenide (CIGS) solar cells with various buffer layers by SCAPS, *Current Applied Physics*, 10 (2010) S387-S391.

[6] Espinel, E., Rojas, J., Florez, E., 2D Simulation of Two-Phase Flow for Water Jet Cutting Processes with OpenFOAM®, (2021) *International Review on Modelling and Simulations (IREMOS)*, 14 (4), pp. 301-310.
doi: https://doi.org/10.15866/iremos.v14i4.19332

[7] Al-Shawesh, Y., Lim, S., Nujaim, M., Analysis of the Design Calculations for Electrical Earthing Systems, (2021) *International Review of Electrical Engineering (IREE)*, 16 (2), pp. 104-117.
doi: https://doi.org/10.15866/iree.v16i2.16839

[8] Cardenas, J., Pabón, J., Rojas, J., CFD Study of Industrial Safety Valves in a Virtual Environment with OpenFOAM® Software, (2020) *International Review of Mechanical Engineering (IREME)*, 14 (11), pp. 674-683.
doi: https://doi.org/10.15866/ireme.v14i11.19031

[9] El Arabi, I., Chafi, A., Kammouri Alami, S., Modeling and Simulation of Transport and Biological Reaction in Fluid-Saturated Porous Media, (2022) *International Review on Modelling and Simulations (IREMOS)*, 15 (3), pp. 197-202.
doi: https://doi.org/10.15866/iremos.v15i3.21884

[10] D. Akrour, M. Tribeche, D. Kalache, A theoretical and numerical study of thermosolutal convection: stability of a salinity gradient solar pond, *Thermal Science*, 15 (2011) 67-80.

[11] K. Decock, S. Khelifi, M. Burgelman, Modelling multivalent defects in thin film solar cells, *Thin Solid Films*, 519 (2011) 7481-7484.

[12] J. Verschraegen, M. Burgelman, Numerical modeling of intra-band tunneling for heterojunction solar cells in SCAPS, *Thin Solid Films*, 515 (2007) 6276-6279.

[13] M. Burgelman, J. Verschraegen, S. Degrave, P. Nollet, Modeling thin-film PV devices, *Progress in Photovoltaics: Research and Applications*, 12 (2004) 143-153.

[14] Farooq, W., Musarat, M., Alaloul, W., Kazmi, S., Altaf, M., Rabbani, M., Comparative Study of Thin-Film Perovskite Solar Cells Based on Methylammonium Lead Iodide and Methylammonium Lead Bromide, (2021) *International Review of Electrical Engineering (IREE)*, 16 (6), pp. 587-595.
doi: https://doi.org/10.15866/iree.v16i6.20189

[15] Zyoud, S., Zyoud, A., Effect of Absorber (Acceptor) and Buffer (Donor) Layers Thickness on Mo/CdTe/CdS/ITO Thin Film Solar Cell Performance: SCAPS-1D Simulation Aspect, (2021) *International Review on Modelling and Simulations (IREMOS)*, 14 (1), pp. 10-17.
doi: https://doi.org/10.15866/iremos.v14i1.19953

[16] Zyoud, S., Zyoud, A., Abdelkader, A., Ahmed, N., Numerical Simulation for Optimization of ZnTe-Based Thin-Film Heterojunction Solar Cells with Different Metal Chalcogenide Buffer Layers Replacements: SCAPS-1D Simulation Program, (2021) *International Review on Modelling and Simulations (IREMOS)*, 14 (2), pp. 79-88.
doi: https://doi.org/10.15866/iremos.v14i2.19954

[17] S.H. Zyoud, A.H. Zyoud, N.M. Ahmed, A.R. Prasad, S.N. Khan, A.F. Abdelkader, M. Shahwan, Numerical modeling of high conversion efficiency FTO/ZnO/CdS/CZTS/MO thin film-based solar cells: Using SCAPS-1D software, *Crystals*, 11 (2021) 1468.

[18] S.H. Zyoud, A.H. Zyoud, N.M. Ahmed, A.F. Abdelkader, Numerical modelling analysis for carrier concentration level optimization of CdTe heterojunction thin film–based solar cell with different non–toxic metal chalcogenide buffer layers replacements: using SCAPS–1D software, *Crystals*, 11 (2021) 1454.

[19] J. Guan, *Synthesis and structural characterization of ZnTe/ZnSe core/shell tunable quantum dots*, in, Massachusetts Institute of Technology, 2008.

[20] S. Saha, M. Johnson, F. Altayaran, Y. Wang, D. Wang, Q. Zhang, Electrodeposition Fabrication of Chalcogenide Thin Films for Photovoltaic Applications, *Electrochem*, 1 (2020) 286-321.

[21] M. Akhsassi, A. El Fathi, N. Erraissi, N. Aarich, A. Bennouna, M. Raoufi, A. Outzourhit, Experimental investigation and modeling of the thermal behavior of a solar PV module, *Solar Energy Materials and Solar Cells*, 180 (2018) 271-279.

[22] Delfianti, R., Nusyura, F., Priyadi, A., Abadi, I., Soeprijanto, A., Optimizing the Price of Electrical Energy Transactions on the Microgrid System Using the Shortest Path Solution, (2022) *International Review on Modelling and Simulations (IREMOS)*, 15 (4), pp. 279-286.
doi: https://doi.org/10.15866/iremos.v15i4.22712

[23] D. Covill, A. Blayden, D. Coren, S. Begg, Parametric finite element analysis of steel bicycle frames: the influence of tube selection on frame stiffness, *Procedia Engineering*, 112 (2015) 34-39.

[24] U. Kingsley, P.E. Imoisili, D. Adgidzi, Finite element analysis of bamboo bicycle frame, *Journal of Advances in Mathematics and Computer Science*, (2015) 583-594.

[25] Hassouna, F., Tubaileh, M., Road Traffic Casualties in West Bank: Trends Analysis and Modeling, (2021) *International Review of Civil Engineering (IRECE)*, 12 (2), pp. 101-107.
doi: https://doi.org/10.15866/irece.v12i2.19907

[26] Romero Garcia, G., Florez Solano, E., Cardenas, J., Experimental and CFD Characterization of the Jacket Vessel Heat Transfer Process, (2020) *International Review on Modelling and Simulations (IREMOS)*, 13 (5), pp. 329-336.
doi: https://doi.org/10.15866/iremos.v13i5.18882

[27] Orjuela Abril, S., Acevedo, C., Cardenas Gutierrez, J., Computational Fluid Dynamics Analysis of Combined Cycle Power Plant Heat Exchanger with OpenFOAM® Software, (2020) *International Review on Modelling and Simulations (IREMOS)*, 13 (5), pp. 319-328.
doi: https://doi.org/10.15866/iremos.v13i5.18891

[28] Espinel, E., Cardenas, J., Romero, G., Sensitivity Analysis Applied to the Thermodynamic Diagnosis of Combustion in a Diesel Engine with DIAGNO-DIESEL® Software, (2020) *International Review of Mechanical Engineering (IREME)*, 14 (6), pp. 395-405.
doi: https://doi.org/10.15866/ireme.v14i6.19101

[29] P.C. Marchal, J.G. Ortega, J.G. García, *Production Planning, Modeling and Control of Food Industry Processes*, Springer, 2019.

[30] H. Biemans, L. Speelman, F. Ludwig, E. Moors, A. Wiltshire, P. Kumar, D. Gerten, P. Kabat, Future water resources for food production in five South Asian river basins and potential for adaptation-A modeling study, *Science of the Total Environment*, 468 (2013) S117-S131.

[31] R. Younas, H. Imran, S.I.H. Shah, T.M. Abdolkader, N.Z. Butt, Computational modeling of polycrystalline silicon on oxide

Copyright © 2023 The Authors. Published by Praise Worthy Prize S.r.l.

passivating contact for silicon solar cells, *IEEE Transactions on Electron Devices*, 66 (2019) 1819-1826.
[32] S. Fantacci, F. De Angelis, Ab initio modeling of solar cell dye sensitizers: The hunt for red photons continues, *European Journal of Inorganic Chemistry*, 2019 (2019) 743-750.
[33] A. Verma, P. Asthana, Modeling of thin film solar photovoltaic based on ZnO/SnS Oxide-absorber substrate configuration, *International Journal of Engineering Research and Applications* 4(6):12-18.
[34] A. Tyagi, K. Ghosh, A. Kottantharayil, S. Lodha, An analytical model for the electrical characteristics of passivated Carrier-Selective Contact (CSC) solar cell, *IEEE Transactions on Electron Devices*, 66 (2019) 1377-1385.
[35] A. Haddout, A. Raidou, M. Fahoume, A review on the numerical modeling of CdS/CZTS-based solar cells, *Applied Physics A*, 125 (2019) 124.
[36] H. Movla, Optimization of the CIGS based thin film solar cells: Numerical simulation and analysis, *Optik*, 125 (2014) 67-70.
[37] A. Luque, S. Hegedus, *Photovoltaic science and engineering*, Wiley Online Library, 2003.
[38] H. Ullah, B. Marí, H.N. Cui, Investigation on the effect of Gallium on the efficiency of CIGS solar cells through dedicated software, in: Applied Mechanics and Materials, *Trans Tech Publ*, 2014, pp. 1497-1501.
[39] N. Paudel, K. Wieland, A. Compaan, Ultrathin CdS/CdTe solar cells by sputtering, *Solar Energy Materials and Solar Cells*, 105 (2012) 109-112.
[40] P. Singh, N.M. Ravindra, Temperature dependence of solar cell performance-an analysis, *Solar energy materials and solar cells*, 101 (2012) 36-45.
[41] S. S. Hegedus, W.N. Shafarman, Thin-film solar cells: device measurements and analysis, *Progress in Photovoltaics: Research and Applications*, 12 (2004) 155-176.
[42] N. Amin, M. Matin, M. Aliyu, M. Alghoul, M. Karim, K. Sopian, Prospects of back surface field effect in ultra-thin high-efficiency CdS/CdTe solar cells from numerical modeling, *International journal of photoenergy*, 2010 (2010).
[43] N. Amin, A. Yamada, M. Konagai, Effect of ZnTe and CdZnTe Alloys at the Back Contact of 1-μm-Thick CdTe Thin Film Solar Cells, *Japanese journal of applied physics*, 41 (2002) 2834.
[44] T. Aramoto, S. Kumazawa, H. Higuchi, T. Arita, S. Shibutani, T. Nishio, J. Nakajima, M. Tsuji, A. Hanafusa, T. Hibino, 16.0% efficient thin-film CdS/CdTe solar cells, *Japanese Journal of Applied Physics*, 36 (1997) 6304.
[45] T. Gessert, P. Sheldon, X. Li, D. Dunlavy, D. Niles, R. Sasala, S. Albright, B. Zadler, Studies of ZnTe back contacts to CdS/CdTe solar cells, in: *Conference Record of the Twenty Sixth IEEE Photovoltaic Specialists Conference*-1997, IEEE, 1997, pp. 419-422.
[46] S. Hossain, N. Amin, M. Martin, M.M. Aliyu, T. Razykov, K. Sopian, A Numerical Study on the Prospects of High Efficiency Ultra Thin Zn x Cd 1-x S/CdTe Solar Cell, *Chalcogenide Letters*, 8 (2011).
[47] Y.-J. Lee, J.L. Gray, Numerical modeling of polycrystalline CdTe and CIS solar cells, in: *Conference Record of the Twenty Third IEEE Photovoltaic Specialists Conference*-1993 (Cat. No. 93CH3283-9), IEEE, 1993, pp. 586-591.
[48] W. Wang, J. Phillips, S. Kim, X. Pan, ZnO/ZnSe/ZnTe heterojunctions for ZnTe-based solar cells, *Journal of electronic materials*, 40 (2011) 1674-1678.
[49] A.A.A. Al-Khazzar, Behavior of four Solar PV modules with temperature variation, *International journal of renewable energy research*, 6 (2016).
[50] A. Sproul, M. Green, Improved value for the silicon intrinsic carrier concentration from 275 to 375 K, *Journal of applied physics*, 70 (1991) 846-854.
[51] A. Sproul, M. Green, Intrinsic carrier concentration and minority-carrier mobility of silicon from 77 to 300 K, *Journal of Applied Physics*, 73 (1993) 1214-1225.
[52] T. Nakada, M. Mizutani, 18% efficiency Cd-free Cu (In, Ga) Se2 thin-film solar cells fabricated using chemical bath deposition (CBD)-ZnS buffer layers, *Japanese Journal of Applied Physics*, 41 (2002) L165.
[53] L. Wang, J. Jin, C. Mi, Z. Hao, Y. Luo, C. Sun, Y. Han, B. Xiong, J. Wang, H. Li, A review on experimental measurements for understanding efficiency droop in InGaN-based light-emitting diodes, *Materials*, 10 (2017) 1233.
[54] S.H. Zyoud, A. Abdelkader, A.H. Zyoud, *The Impact of Temperature on the Performance of Semiconductor Laser Diode*, (2020).
[55] S. Adachi, *Properties of semiconductor alloys: group-IV, III-V and II-VI semiconductors*, John Wiley & Sons, 2009.
[56] R. Pässler, Parameter sets due to fittings of the temperature dependencies of fundamental bandgaps in semiconductors, *Physica Status Solidi* (b), 216 (1999) 975-1007.
[57] B. Xiao, M. Zhu, B. Zhang, J. Dong, L. Ji, H. Yu, X. Sun, W. Jie, Y. Xu, Optical and electrical properties of vanadium-doped ZnTe crystals grown by the temperature gradient solution method, *Optical Materials Express*, 8 (2018) 431-439.

Authors' information

[1]Department of Mathematics and Sciences, Ajman University, Ajman, United Arab Emirates.

[2]Nonlinear Dynamics Research Center (NDRC), Ajman University, Ajman, United Arab Emirates.

[3]Department of Chemistry, An-Najah National University, Nablus, Palestine.

Samer H. Zyoud was born in Palestine, received the B.Sc. degree in physics from University of Mosul, Al- Mosul, Iraq, in 2001, the M.Sc. degree in physics from University of Baghdad, Baghdad, Iraq, in 2003, at present, he has been working as senior lecturer at Ajman University, Ajman, United Arab Emirates and PhD Student at University Sains Malaysia, Penang, Malaysia. Research area: Nanostructures Thin Film - based (Solar cell, Photocatalyst, Sensor) and semiconductor laser with application.
Email: s.zyoud@ajman.ac.ae

Ahed H. Zyoud (Corresponding Author) was born at Seilat Al-Harthiya/Jenin in 1973, received the B.Sc. at the Yarmouk University, Jordan in 1996, M.Sc. at An-Najah National University, Palestine in 2000, and the Ph.D. at An-Najah National University, Palestine in 2009. Zyoud is a professor at An-Najah national university, Chemistry department. His research activity is focused on material and nanotechnology, preparation, and characterization. Applications of the prepared nanomaterials in the fields of thin-film photovoltaic application in addition photodegradation of water organic contaminants.
E-mail: ahedzyoud@najah.edu